

Role of grain boundary networks in vortex motion in superconducting films

Yu Liu(刘宇), Feng Xue(薛峰), and Xiao-Fan Gou(苟晓凡)
Citation: Chin. Phys. B, 2023, 32 (**12**): 127401. DOI: 10.1088/1674-1056/ace315
Journal homepage: http://cpb.iphy.ac.cn; http://iopscience.iop.org/cpb

What follows is a list of articles you may be interested in

Anisotropic superconducting properties of $FeSe_{0.5}Te_{0.5}$ single crystals

Jia-Ming Zhao(赵佳铭) and Zhi-He Wang(王智河)
Chin. Phys. B, 2022, 31 (**9**): 097402. DOI: 10.1088/1674-1056/ac5610

Barrier or easy-flow channel: The role of grain boundary acting on vortex motion in type-II superconductors

Yu Liu(刘宇), Xiao-Fan Gou(苟晓凡), and Feng Xue(薛峰)
Chin. Phys. B, 2021, 30 (**9**): 097402. DOI: 10.1088/1674-1056/ac11ea

Multiple reversals of vortex ratchet effects in a superconducting strip with inclined dynamic pinning landscape

An He(何安) and Cun Xue(薛存)
Chin. Phys. B, 2020, 29 (**12**): 127401. DOI: 10.1088/1674-1056/abbbe5

Time-dependent Ginzburg-Landau equations for multi-gap superconductors

Minsi Li(李敏斯), Jiahong Gu(古家虹), Long Du(杜龙), Hongwei Zhong(钟红伟), Lijuan Zhou(周丽娟), Qinghua Chen(陈庆华)
Chin. Phys. B, 2020, 29 (**3**): 037401. DOI: 10.1088/1674-1056/ab69ef

Critical current density behaviors across a grain boundary inclined to current with different angles in $YBa_2Cu_3O_{7-\delta}$ bicrystal junctions

Tao Hua(花涛), Wei-Wei Xu(许伟伟), Zheng-Ming Ji(吉争鸣), Da-Yuan Guo(郭大元), Qing-Yun Wang(王青云), Xiang-Rong Ma(马湘蓉), Rui-Yu Liang(梁瑞宇)
Chin. Phys. B, 2016, 25 (**6**): 067401. DOI: 10.1088/1674-1056/25/6/067401

Role of grain boundary networks in vortex motion in superconducting films

Yu Liu(刘宇), Feng Xue(薛峰), and Xiao-Fan Gou(苟晓凡)[†]

College of Mechanics and Materials, Hohai University, Nanjing 211100, *China*

(Received 18 April 2023; revised manuscript received 19 June 2023; accepted manuscript online 30 June 2023)

We study the vortex dynamics of the polycrystalline superconductors in the presence of both random point defects and the generated grain boundary (GB) networks with Voronoi diagram. The synergistic effect of adjacent GBs on restricting the vortex motion in intragranular region is proposed and the corresponding intensity factor of the synergistic effect which characterizes the strength of the synergistic restriction of adjacent grain boundaries is also determined in the present work. The interconnected GBs offer easy-flow channels for vortices in addition to pinning effects on the vortices. The combined channels and the vortex flow patterns in the superconducting film are analyzed in detail from molecular dynamics simulations. Furthermore, it is discovered that the critical current increases with the decrease of magnetic field intensity, temperature, and the average grain size. The large number of vortices results in the enhanced repulsive interaction forcing the vortices to move out from the GBs. The thermal depinning from GBs leads to the lower Lorentz force range. The increase of the grain size causes the number of GBs to decrease. In summary, these effects leads the critical current to become a decreasing function of magnetic field, temperature, and grain size.

Keywords: grain boundary network, Voronoi tessellation, synergistic effect, intensity factor of synergistic effect, vortex motion, combined channels

PACS: 74.25.Wx, 74.72.–h, 74.78.–w **DOI:** 10.1088/1674-1056/ace315

1. Introduction

In the mixed state of high-T_c superconductors, the quantized magnetic flux, viz. vortex lines, penetrates into the sample. The motion of the vortices driven by an external electric current leads to the associated Ohmic loss, increasing the resistivity of the superconductor. To preserve the material' superconductivity, it is imperative to impede the current-induced motion of the vortices. Pinning plays a crucial role in determining the vortex dynamics in the mixed state of type-II superconductors, which is important for lossless transport in the applications of superconductors.[1–9] It has been suggested to introduce many defects as effective pinning centers against the driving force of magnetic flux flow. Of them, twin boundaries may be the most significant anisotropic pinning defects in the cuprate compound $YBa_2Cu_3O_{7-x}$ (YBCO). Because of the importance and attraction of grain boundaries, with the development of technology in this field, various theoretical calculations and experiments have been performed.[10–20] The effect of grain boundaries on critical current density was indicated by using the techniques of magneto-optical measurements and magnetic hysteresis measurements. From acting as easy flow pathways for longitudinal vortex motion and serving as barriers for transverse vortex motion to angular dependence of vortex motion relative to the grain boundary, the understanding of the GB behavior has been gradually improved.[21–23]

Although numerous studies of thin films and bulk samples have evaluated the influence of grain boundaries (GBs) on vortex motion, they mainly focused on the circumstances of parallel GBs or a single GB.[22–25] As is well known, the role of the GB which can be changed from a barrier to an easy-flow channel is intrinsically determined by the competitive effect associated with the action on vortex between in the GB and intragranular region, and also affected by the angle between the grain boundary and the applied current based on previous work.[26] The investigations on random GB networks with complex orientations which can model polycrystalline materials also play a crucial role in gaining a deeper knowledge about grain boundary mechanism on vortex motion.[27,28] In the present work, the GB networks are generated in the coordinates of the nuclei of crystals by using Voronoi tessellation. In order to study the vortex dynamics in superconducting films, the GB is assumed to be composed of uniformly distributed special sites and an attraction well formed by the local electric fields. The synergistic effect of GB networks on vortex motion is introduced in detail. Besides, the effects of flux flow channel networks on vortex motion in the GB region formed in the depinning transition process are presented. In the next section, the influence of the magnetic field intensity, temperature, and the grain boundary density (or grain size) on the vortex flow patterns and transportation properties are discussed by analyzing the average vortex velocity and the Lorentz force which are related to macroscopically measured voltage and current respectively.

[†]Corresponding author. E-mail: xfgou@hhu.edu.cn

© 2023 Chinese Physical Society and IOP Publishing Ltd

2. Calculation model and approach

2.1. Model for GB networks

A series of random numbers that play a role in nucleation on crystal is generated in a given finite area. The Delaunay triangle is formed by triangles that do not contain any other points within the circumscribed circle of three vertices as shown in Fig. 1. The circumcenter of the Delauny triangles are called Voronoi points. The grain boundaries are created through the coordinates of the nuclei of the crystals by employing Voronoi tessellation.[29–32] Figures 2(a) and 2(b) show the simulation results for the cases of the 10 grains and 20 grains generated, respectively. Considering the periodic boundary conditions required in the following calculations, the coordinates of the intersection points between the boundaries and the GBs are appropriately adjusted according to the symmetry. The average grain size is approximately 7λ in Fig. 2(a) and 5λ in Fig. 2(b), while the model size is selected as $20\lambda \times 20\lambda$.

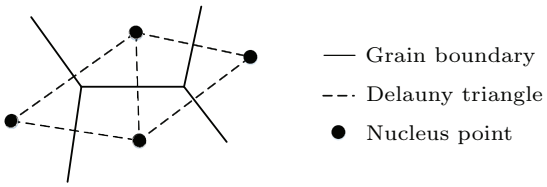


Fig. 1. Delauny triangle and Voronoi tessellation.

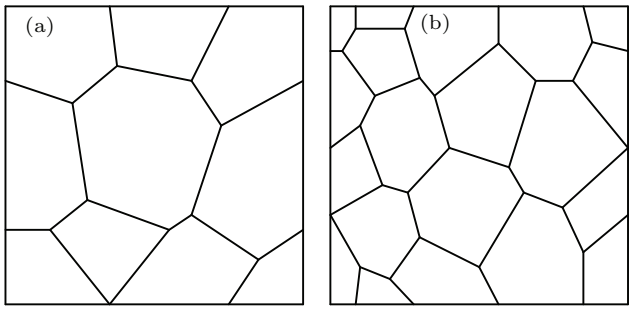


Fig. 2. Microstructure samples by Voronoi tessellation for (a) 10 grains and (b) 20 grains.

2.2. Model for vortex dynamics

The geometric structure we simulate is an infinite superconducting slab containing the GB networks with random angles, which belongs to the category of two-dimensional (2D) periodic system. According to previous researches,[26] the GBs are modelled as the potential wells, because the behavior of the vortices in the vicinity of the GB is similar to the motion of charge carriers caused by the electric field. We assume that the GB is composed of a series of dislocations (red dots) distributed along the GB and the local electric fields applied to the specific areas, normal to the direction of the GB as shown in Fig. 3. The vortices moving into the specific areas would be subjected to an additional electric force whose direction is perpendicular to the GB and always points to the GB region since the local electric fields on both sides of the GB are identical in magnitude but opposite in direction.

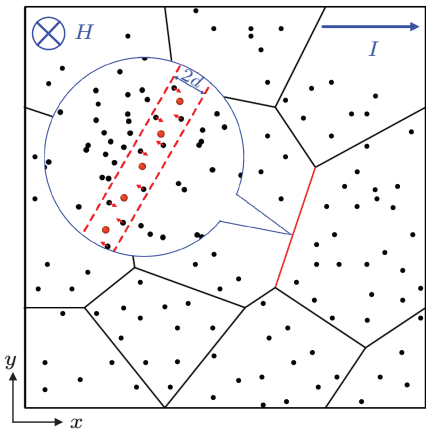


Fig. 3. Calculation model showing a magnetic vortex pinning area of type-II polycrystalline superconductors with GB networks. The red magnified area represents the GB model and the GB is modeled as an attractive well, $2d$ is the effective width of the GB and d is taken as 0.15λ.[22,24,28] In the GB region, a series of red dots indicates dislocations, and the red arrows acting on vortices denote the directions of electric forces. H and I refer to the applied magnetic field and transport current, respectively.

We study $N_{\rm v}$ Abrikosov vortices interacting with GB networks described above and $N_{\rm p}$ random pining centers in a 2D slice in the x–y rectangular system of the three-dimensional (3D) slab. Periodic boundary conditions are used for the x axis direction and y axis direction. The orientation of the applied current is taken along the x axis. Taking the London limit $\lambda_{\rm L} \gg \xi_{\rm s}$ into account, the vortices can be regarded as point particles where $\lambda_{\rm L}$ is the penetration length and $\xi_{\rm s}$ is the superconducting coherence length. In the present work, the LAMMPS molecular dynamics code is employed to conduct the numerical calculation.

The equation of the time evolution of a vortex i at a position r_i can be written as[33,34]

$$m\frac{{\rm d}^2 r_i}{{\rm d}t^2}+\eta\frac{{\rm d}r_i}{{\rm d}t} = -\sum_{j\neq i}\nabla_i U^{\rm vv}(r_{ij})-\sum_{p}\nabla_i U^{\rm vp}(r_{ij})+F_{\rm L}+F_i^{\rm th}(t)+F_{\rm GB}, \quad (1)$$

where r_{ip} is the distance between the vortex i located at r_i and the pinning site located at r_p, r_{ij} is the distance between the vortices i and j, and ∇_i is the gradient operator acting on r_i, η and m are the viscosity coefficient and the vortex mass, and $m/\eta = 0.1$ is so chosen that the inertial term which is proportional to the particle mass is small enough compared with the viscous term in the second-order Newton's vortex dynamics. Such a ratio can ensure that the results possess the same reliability as those from the overdamped equation which is used for the superconductor vortices. $F_{\rm L}$ is the Lorentz force caused by an applied current and is given by $F_{\rm L} = J \times \Phi_0$,[2,23] where J is the external current density and Φ_0 is the magnetic flux quantum. All vortices are considered to be subjected to the

Lorentz force in the same way. $F_i^{\rm th}$ is the Langevin force described by the thermal Gaussian white noise with zero mean and variance[33,34]

$$\langle F_{i,\lambda}^{\rm th}(t)F_{j,\mu}^{\rm th}(t')\rangle = 2\eta k_{\rm B}T\delta_{ij}\delta_{\lambda\mu}\delta\left(t-t'\right), \tag{2}$$

where $k_{\rm B}$ is the Boltzmann constant, T is the temperature, and λ, $\mu = x, y$. The vortex–vortex repulsive interaction is determined by a modified Bessel function[33,34]

$$U^{\rm vv}(r_{ij}) = \alpha_{\rm v}{\rm K}_0(r_{ij}/\lambda_{\rm L}), \tag{3}$$

and the attractive pinning potential is given by[33,34]

$$U^{\rm vp}(r_{ip}) = -\alpha_{\rm p}\,{\rm e}^{-\left(r_{ip}/R_{\rm p}\right)^2}, \tag{4}$$

where $\alpha_{\rm p}$ and $\alpha_{\rm v}$ are the tunable parameters, and $R_{\rm p}$ is the radius of the pins. The $F_{\rm GB}$ is the GB force acting on the vortices and it includes the influence of the local electric field described above and the effect of a series of dislocations acting as special uniform pinning centers. The related parameters E (the electric field intensity) and q (charge of the vortices) are tunable parameters. The pinning potential of the special pins along the GB is determined by[26]

$$U^{\rm vs}(r_{ip}) = -\beta\alpha_{\rm p}\,{\rm e}^{-\left(r_{ip}/R_{\rm p}\right)^2}, \tag{5}$$

where β is a tunable coefficient. The influence of the local electric field occurs when the vortices move into the specified areas in the vicinity of the GB, and disappears after the vortices have moved out of the areas. In fact, the form of vortex–vortex repulsive interaction in Eq. (3) can be derived from the London theory, and the coefficient $\Phi_0^2/(8\pi^2\lambda_{\rm L}^2)$ is adjusted to the parameter $\alpha_{\rm p}$ with a characteristic energy per unit length $\varepsilon_0 = (\Phi_0/(4\pi\lambda_{\rm L}))^2$.[35] We cut off the long-range interaction force at $6.5\lambda_{\rm L}$ since the modified Bessel function ${\rm K}_1$ decays quickly.[24,34] The radius of the pin is $R_{\rm p} = 0.22\lambda_{\rm L}$, which is comparable to the vortex superconducting coherence length.[34] We use a unit system in which $\eta = 1$, $\lambda_{\rm L} = 1$, $\varepsilon_0 = 1$, and $k_{\rm B} = 1$.

3. Results and discussion

3.1. Synergistic effect of adjacent GBs on limiting the vortex motion in no-GB region

As is well known, the effect of grain boundary on vortices is derived from vortices trapped in the grain boundary region serving as an initial potential well on vortices in the intragranular region, as shown in Fig. 4(a). Within the coverage range of the cutoff radius, the force exerted by the grain boundary on the vortex in the no-GB region can be expressed as

$$F_{\rm gv} = \sum_{i=1}^{n} F_i. \tag{6}$$

"Y"-type structure can be selected as a typical sample to analyze the combined influence of adjacent grain boundaries as depicted in Fig. 4(b). The overall force exerted by neighboring grain boundaries on the vortex in no-GB region can be written as

$$F_{\rm Gv} = F_{\rm gv1} + F_{\rm gv2}. \tag{7}$$

The aforementioned Eqs. (6) and (7) demonstrate that there is a synergistic limitation influence on the vortex in no-GB region by the adjacent grain boundaries. In addition, equation (3) shows that the force exerted by a single trapped vortex on a vortex in no-GB region is inversely proportional to that the distance of the vortex from the grain boundary. In conclusion, the distance between the vortex in no-GB region and the grain boundary can indicate the strength of the synergistic effect of the adjacent GBs. Keeping d_1 (the distance between the vortex in no-GB region and the grain boundary 1, as shown in Fig. 4(b)) constant, the distance of the vortex from another neighboring grain boundary 2 is given by

$$d_2 = l\sin\theta_2, \tag{8}$$

where l is the distance from the vortex in no-GB region to the intersection of adjacent grain boundaries. The changes in θ_2 and θ are consistent when θ_1 is fixed.

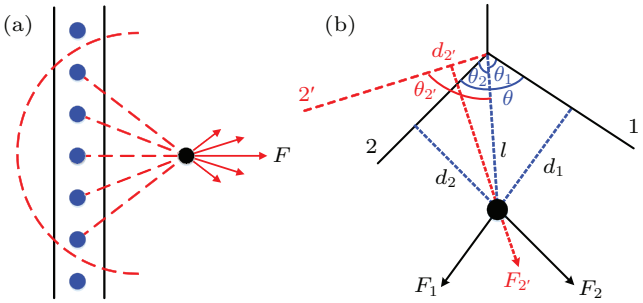


Fig. 4. (a) Repulsive effect of trapped vortices in GB region on vortices in no-GB region in the coverage range of the cutoff radius, and (b) synergistic restriction on the vortex from the adjacent grain boundaries.

The intensity factor of the synergistic effect is defined as

$$\gamma = \frac{1}{d_2} = \frac{1}{l\sin\theta_2}, \tag{9}$$

where γ characterizes the strength of the synergistic restriction of adjacent grain boundaries on vortex in no-GB region.

Firstly, the strength of the synergistic effect varying with the angle between the adjacent GBs and with the distance from the intersection point of nearby GBs to the vortex are calculated. As shown in Fig. 5(a), the intensity factor γ decreases as the angle θ between adjacent GBs increases. The angle corresponds to grain size, in other words, the smaller the gain size, the stronger the synergistic effect is. It should be noted that the strength of synergistic effect is no longer determined by the distance of the vortex from the grain boundary while the angle θ_2 exceeds 90°. After θ_2 reaches to 90°, the nominal distance between the vortex and the grain boundary decreases, while

the actual distance between them expands, and the strength of the limiting effect correspondingly declines. From Fig. 5(b), it can be seen that the intensity factor γ declines with distance l increasing. That is to say, the restriction is strengthened with the vortex approaching to the grain boundary. In summary, the synergistic effect strength of adjacent GBs on limiting the vortex motion in no-GB region is negatively related to the angle of adjacent grain boundaries and the distance from vortex to the grain boundaries, viz. The stronger synergistic restriction effect on vortex in no-GB region results from smaller grain sizes and closer distance between the vortex and the grain boundaries.

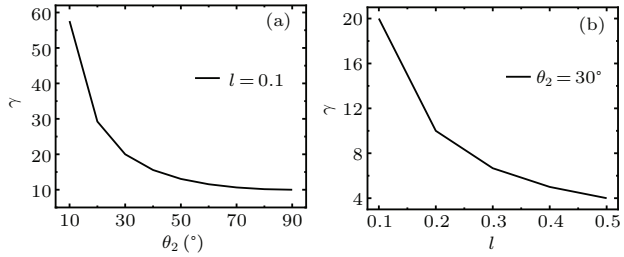


Fig. 5. The intensity factor γ versus (a) angle θ of adjacent grain boundaries and (b) distance from the intersection of neighboring grain boundaries to the vortex in no-GB region, respectively, with θ_1 fixed at 30°.

3.2. Effect of combined channels and flow channel networks on vortex motion in GB region

In the depinning transition process, easy-flow channels will be formed between adjacent grain boundaries as shown in Fig. 6(a). With the Lorentz force increasing, more grain boundaries form part of the interconnection network as shown in Fig. 6(b). In this complex network, it can be found that the flow path of vortex is related to the angle between the current direction and the grain boundary. When the grain boundary tends to be parallel to the current direction, the grain boundary restricts the vortex flow strongly, which is not conducive to the formation of channels. Consequently, unlike point pinning centers, the interconnected GBs provide easy-flow pathways in addition to pinning effect on the vortices.

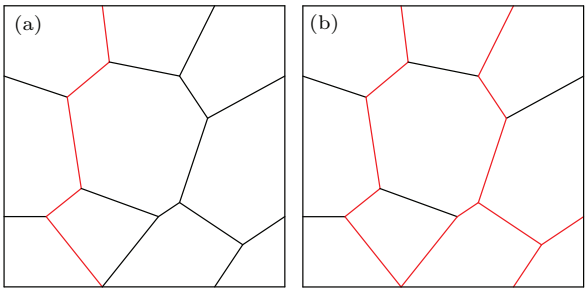


Fig. 6. (a) Combined channels formed by adjacent grain boundaries, (b) Influence of the angular relationship between grain boundary and vortex direction on combined channel.

3.3. Typical flow patterns in the superconducting film at different applied magnetic fields

By varying the Lorentz force, the flowing states of the vortices in the sample with the random GB network are simulated. Both the large average grain size 7λ and the small average grain size 5λ are taken into account, and the random GB network structure with the former one is chosen to illustrate the flux flow condition under various magnetic fields. At low magnetic field, vortices flow along the GBs when the Lorentz force exceeds the critical depinning force F_c over which the system begins to slid from a pinned state as demonstrated in Fig. 7(a). With applied current increasing, the vortices can escape from the GBs, viz. transfer from one grain to another across the GB as shown in Fig. 7(b). At higher magnetic field, the depinning behavior occurs at a certain threshold current, specifically, the vortices in GB region flow slowly along the GB and the vortices in no-GB region do not move out just as represented in Fig. 7(c). When the applied current is large enough, the vortices move across the GBs and all vortices move quickly along the direction of the Lorentz force as shown in Fig. 7(d). The flow patterns and typical trajectories in our work accord with the results in Refs. [22,27].

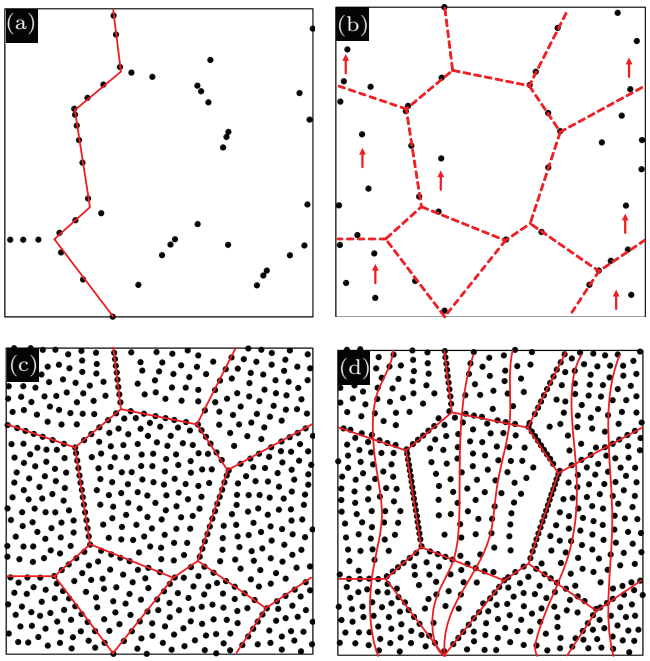


Fig. 7. Typical flow trajectories (red lines) for $N_v = 48$ (a) in initial state of vortices (black dots) moving along the GBs and (b) in state of vortices escaping from GBs, and for $N_v = 460$ (c) in stage of vortices flow slowly along the GB networks and (d) in stage of vortices moving fast along the direction of the Lorentz force, with dash lines representing the position of GB networks and the red arrows showing the vortices moving across the GBs.

3.4. Influence of N_v, T, and average grain size on transport properties in compound YBCO

The macroscopic current–voltage properties of the YBCO conductors can be described by the relationship between the average velocity v_y and the driving force F_L. Accordingly, the variations of the average velocity v_y with the driving force F_L in three cases of the magnetic field: $N_v = 115$, 230, and 460 for the samples at $T = 0$ K, and 10 grains, 20 grains or no GB, respectively, are used to observe correspondingly diverse

current–voltage properties. As shown in Fig. 8, the average velocity v_y increases when the Lorentz force exceeds the critical driving force, which implies that the unpinned vortices move into the flow state. The threshold of the vortex motion shifts into the higher Lorentz force range as the vortex number decreases, this indicates that the critical current increases as the magnetic field intensity decreases. The removal of vortices from the GBs is thought to be the cause of this behavior owing to the enhanced repulsive force caused by a large number of vortices.

In addition, the effect of temperature on current–voltage characteristics in the superconducting film is also important. Therefore, the relationships of the average velocity v_y with the Lorentz force F_L for the samples of 10 grains, and $N_v = 115$, 230 or 460 at temperature $T = 0$ K, 50 K, and 90 K respectively, are given in Fig. 9. The intensity of the v_y fluctuation increases as the temperature rises when the vortices number N_v is relatively small, as illustrated in Fig. 9(a), suggesting that the vortex motion is becoming more disordered and the system tends to be unstable. However, as the density of vortices is increased, the motion of the vortices progressively tends to stabilize as depicted in Figs. 9(b) and 9(c), indicating that the long-range order of the vortices arrangement plays a certain role. The depinning transition process transfers toward the lower Lorentz force range with the temperature increasing, implying that the thermal depinning from GBs occurs more easily.

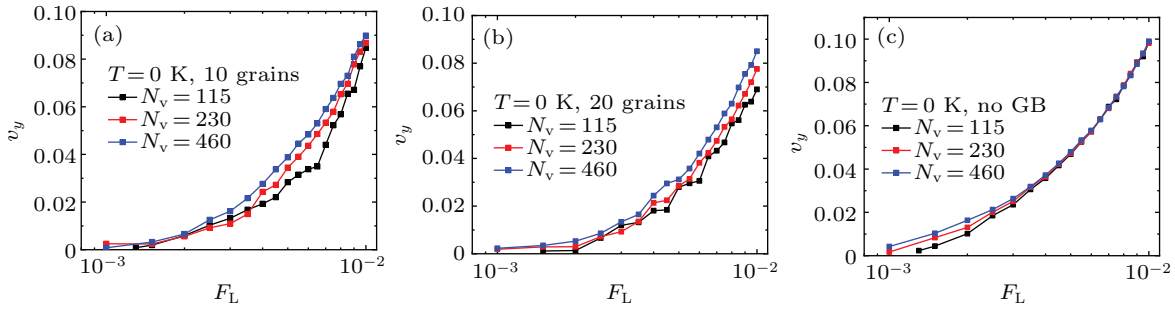


Fig. 8. Variations of the average velocity v_y with Lorentz force in the superconducting film at vortex number N_v of 115, 230, and 460 for $T = 0$ K, and for (a) 10 grains, (b) 20 grains, and (c) no GB.

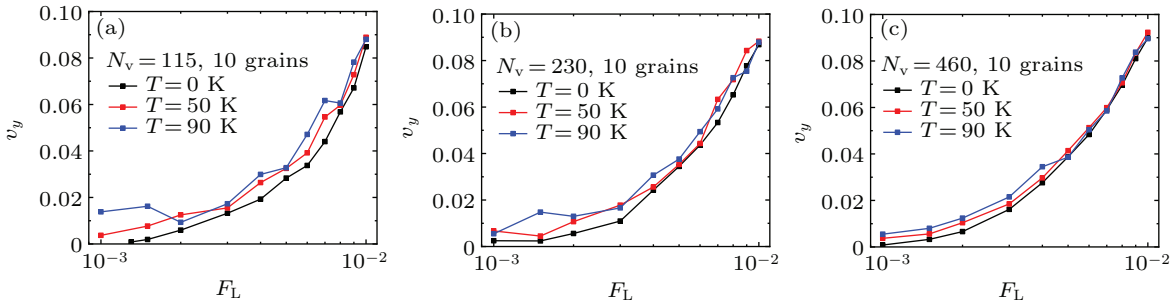


Fig. 9. Variations of the average velocity v_y with Lorentz force in the superconducting film at temperature T of 0 K, 50 K, 90 K for 10 grains, and $N_v = 115$ (a), 230 (b), and 460 (c).

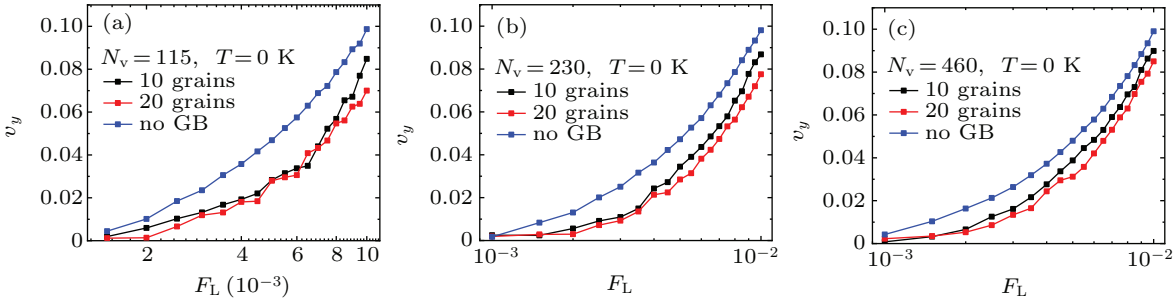


Fig. 10. Variations of average velocity v_y with Lorentz force in superconducting film at different grain sizes of no GB, 10 grains, 20 grains for $T = 0$ K, and $N_v = 115$ (a), 230 (b), and (c) 460.

Finally, the variations of the transport properties with grain size for $T = 0$ K, and $N_v = 115$, 230 or 460, respectively, are discussed in Fig. 10. At a low applied magnetic field, the critical current density increases as the number of GBs pinning centers augments, viz. the grain size decreases. The GB with an angle that is close to a right angle with respect to the direction of vortex motion, plays a barrier role in limiting the motion of vortices. With the decrease of grain size, the number of GBs increases and the orientations of GBs become complicated (including the GBs with large angle relative to the

vortex motion), leading the critical current density to increase. The pinning effect of GB network dominates in a low magnetic field, and the increase of critical current density can be achieved by optimizing the grain size.

In fact, in addition to the grain boundary landscapes used in this work, we also create two other random grain boundary landscapes using Vonoroi diagrams for specific average grain sizes (10 grains and 20 grains), and their simulation results are almost the same because the fluctuation of the calculation values is so small that it cannot change the simulation results. This indicates that with sufficient GBs, the grain boundary orientations tend to be disordered, and the simulated current voltage relationship is a statistical result, which is not substantially related to the grain boundary landscapes randomly.

4. Summary

We have investigated the flux pinning in polycrystalline YBCO with the large-scaled pinning landscape including both point pinning centers and GB networks generated by using the Voronoi method. The synergistic effect of adjacent GBs on limiting vortex motion in intragranular region is proposed, and the intensity factor of the synergistic effect which is associated with the angle between the adjacent GBs and the distance of the intersection point of nearby GBs to the vortex is determined in our work. Then we analyze the vortex flow patterns through the polycrystalline sample with random GB networks. The combined channels formed by adjacent grain boundaries and flow channel networks for vortex motion in GB region are introduced in the depinning transition process. The angle between the vortex motion direction and the grain boundary affects the vortex's flow pathway. The GBs with large angles relative to the vortex motion is incompatible with the development of channels since they limit the vortex flow intensely. Moreover, typical flow patterns driven by the Lorentz force in the superconducting film in different applied magnetic fields in the case of large grain size are discussed in detail. Finally, in order to improve superconducting transport properties, the relationships of the average velocity v_y with the driving force F_{L} are calculated and discussed by varying the magnetic field, temperature, and grain size. The critical current decreases with the augment of magnetic field intensity, which is because the vortices move out through the GBs by the enhanced repulsive force resulting from the large distribution density of vortices. With the increase of temperature, the thermal depinning from GBs results in the lower Lorentz force range. The critical current density increases as the grain size decreases, for the number of GBs increases and the pinning effect of GB network dominates at low magnetic field.

Acknowledgement

Project supported by the National Natural Science Foundation of China (Grant Nos. 12232005 and 12072101).

References

[1] Naito T, Iwasaki H, Nishizaki T and Kobayashi N 2007 *Physica C* **460–462** 1196
[2] Zhu B Y, Xing D Y, Dong J and Zhao B R 1999 *Physica C* **311** 140
[3] Matsumoto K and Mele P 2010 *Supercond. Sci. Technol.* **23** 014001
[4] Reichhardt C and Olson Reichhardt C J 2017 *Rep. Prog. Phys.* **80** 026501
[5] Miller D J, Gray K E, Field M B and Kim D 1999 *IEEE T. Appl. Supercon.* **9** 2030
[6] Chen Z, Yong H and Zhou Y 2018 *Physica C* **552** 22
[7] He A, Xue C and Zhou Y 2018 *Chin. Phys. B* **27** 057402
[8] Gao L X, Zhang X K, Zhang A L, Xiao Q L, Chen F and Ge J Y 2022 *Chin. Phys. B* **32** 037402
[9] Yu A, Huang Z, Zhang C, Wu Y, Wang T, Xie T, Liu C, Li H, Peng W, Luo H and others 2021 *Chin. Phys. B* **30** 027401
[10] Xue F, Gu Y and Gou X 2016 *J. Supercond. Nov. Magn.* **29** 2711
[11] Jooss Ch, Guth K, Born V and Albrecht J 2001 *Phys. Rev. B* **65** 014505
[12] Dıaz A, Mechin L, Berghuis P and Evetts J E 1998 *Phys. Rev. Lett.* **80** 3855
[13] Gurevich A, Rzchowski M S, Daniels G, Patnaik S, Hinaus B M, Carillo F, Tafuri F and Larbalestier D C 2002 *Phys. Rev. Lett.* **88** 097001
[14] Hua T, Xu W, Zhang Y, Jiang L, An D, Shi J, Yu M, Wang Z, Chen J, Kang L, Jin B, Wang H and Wu P 2015 *Supercond. Sci. Technol.* **28** 025005
[15] Inoue M, Kiss T, Koyanagi S, Imamura K, Takeo M, Iijima Y, Kakimoto K, Saitoh T, Matsuda J, Tokunaga Y, Izumi T and Shiohara Y 2005 *Physica C* **426–431** 1068
[16] Albrecht J, Leonhardt S and Kronmueller H 2000 *Phys. Rev. B* **63** 014507
[17] Volodin A, Temst K, Bruynseraede Y, Van Haesendonck C, Montero M I, Schuller I K, Dam B, Huijbregtse J M and Griessen R 2002 *Physica C* **369** 165
[18] Gurevich A 2002 *Phys. Rev. B* **65** 214531
[19] Palau A, Puig T, Gutierrez J, Obradors X and de la Cruz F 2006 *Phys. Rev. B* **73** 132508
[20] Feldmann D M, Holesinger T G, Feenstra R and Larbalestier D C 2008 *J. Am. Ceram. Soc.* **91** 1869
[21] Hua T, Yu M, Geng H, Xu W, Lu Y, Qin C, Yu H, Wu J, Wang H, Chen J and Wu P 2018 *Physica C* **554** 15
[22] Enomoto Y and Mitsuda T 2002 *Physica C* **367** 60
[23] Jiang L, Xu W, Hua T, Yu M, An D, Chen J, Jin B, Kang L and Wu P 2015 *Sci. China Technol. Sci.* **58** 493
[24] Asai H and Watanabe S 2008 *Phys. Rev. B* **77** 224514
[25] Asai H and Watanabe S 2013 *Physica C* **485** 125
[26] Liu Y, Gou X F and Xue F 2021 *Chin. Phys. B* **30** 097402
[27] Ren H X and Xue C 2022 *Supercond. Sci. Technol.* **35** 075001
[28] Enomoto Y and Itamoto H 2003 *Physica C* **392–396** 341
[29] Akiniwa Y, Machiya S, Serizawa K and Tanaka K 2004 *Micro-Nanomechatronics and Human Science,* 2004 *and The Fourth Symposium Micro-Nanomechatronics for Information-Based Society*, 2004, Nagoya, Japan, pp. 75–80
[30] Aurenhammer F 1991 *ACM Comput. Surv.* **23** 345
[31] Aurenhammer F and Klein R 2000 *Handbook of computational geometry* **5** 201
[32] Wang S, Tian Z, Dong K and Xie Q 2021 *J. Alloys Compd.* **854** 156983
[33] Fily Y, Olive E, Di Scala N and Soret J C 2010 *Phys. Rev. B* **82** 134519
[34] Di Scala N, Olive E, Lansac Y, Fily Y and Soret J C 2012 *New J. Phys.* **14** 123027
[35] Kulić M and Rys F S 1989 *J. Low Temp. Phys.* **76** 167